Zhang *et al. Satellite Navigation* (2022) 3:16
https://doi.org/10.1186/s43020-022-00076-0

Satellite Navigation
https://satellite-navigation.springeropen.com/

ORIGINAL ARTICLE Open Access

A resilient adjustment method to weigh pseudorange observation in precise point positioning

Qieqie Zhang[1*], Long Zhao[2] and Jianhua Zhou[3]

Abstract

The accurate weighting of pseudorange observations is important to improve the convergence time and positioning quality of Precise Point Positioning (PPP). Currently, the weight of a pseudorange observation is mainly determined with empirical stochastic models. However, in a complex environment, due to the inability to adapt for the dynamic changes of the user environment, the empirical stochastic models usually cannot reflect the real error level of pseudorange observations. To address this problem, a resilient adjustment method to weigh pseudorange observations is proposed, which constructs the real-time estimation and inflation model for the variance of pseudorange multipath error and measurement noise to replace the empirical stochastic model to determine the weights of pseudorange observations. A set of static and dynamic Global Positioning System (GPS) test data are used to verify the effectiveness of the proposed method. The test results indicate that the proposed real-time estimation model can provide a better representation of the pseudorange accuracy, and the positioning performance of PPP using the real-time estimation model is better than that with the empirical stochastic model. Compared with the optimal empirical stochastic model, the positioning accuracy of PPP with the real-time estimation model is improved by at least 20%, and the convergence time is reduced by at least 50%.

Keywords: Precise point positioning, Stochastic model, Resilient adjustment, Complex environments

Introduction

In a complex environment, due to the influence of various error sources the accuracy of observation data is much related to the observed satellites, especially pseudorange observations. In order to improve the convergence time, positioning reliability and accuracy of Precise Point Positioning (PPP), it is necessary to properly weigh each observation. A stochastic model is used to describe the statistical characteristics of observation errors, which is the key to the determination of the weights of observations (Dovis et al., 2015). Therefore, accurate stochastic model is important for improving the positioning performance.

In order to determine the weights of observations, researchers have proposed a variety of empirical stochastic models, which are usually a function of the satellite elevation angle, signal-to-noise ratio, carrier-to-noise ratio, or multipath factor, to estimate the measurement variance (Parvazi et al., 2020; Zhang et al., 2019a, 2019b). The coefficients of an empirical stochastic model are usually fixed. However, in complex environments, measurement error is related to many factors such as the signal power, the types of receivers and observations, the design of the antenna, the satellite constellation, and the satellite elevation angle (Zhang et al., 2018). Because those factors vary significantly during the process, it is difficult to accurately evaluate the statistical characteristics of the measurement error in real-time by using an empirical

*Correspondence: zhangqieqie@nuaa.edu.cn

[1] College of Automation Engineering, Nanjing University of Aeronautics and Astronautics, Nanjing 211106, China
Full list of author information is available at the end of the article

stochastic model. Therefore, the empirical stochastic model used usually cannot reflect the real error level of observations in complex environments.

To deal with the time-varying and unpredictable observation errors in complex environments, many scholars have carried out extensive research on resilient stochastic models and put forward various resilient adjustment methods (Yang, 2019; Zhang et al., 2020), including Multiple Model Adaptive Estimation (MMAE), Variance Component Estimation (VCE), and covariance matching methods. The MMAE method (Shen et al., 2022) adopts a set of parallel filters with different observation covariance matrices to estimate the state parameters, and then fuses the state estimation according to the a posterior probability of each filter. This method can obtain the optimal state estimation theoretically, but needs to set many parallel filters, which will lead to serious memory resource consumption and affect the real-time performance. The VCE methods include Helmert Variance Component Estimation (HVCE) (Gao et al., 2016), Minimum Norm Quadratic Unbiased Estimator (MINQUE) (Zhang et al., 2019a, 2019b), the Best Invariant Quadratic Unbiased Estimator (BIQUE) (Zhang et al., 2019a, 2019b), and the Least-square Variance Component Estimator (LS-VCE) (Parvazi et al., 2020). They generally use the residuals to estimate the (co)variance of observations, which requires a lot of redundant observations to obtain reliable (co) variances. Therefore, the VCE methods are mainly used for post-processing analysis or to determine the scale factors of different types or groups of observations (Parvazi et al., 2020; Zhang et al., 2019a, 2019b). The covariance matching methods include the Residual-based Adaptive Estimation (RAE) (Lee et al., 2020) and the Innovation-based Adaptive Estimation (IAE) (Liu et al., 2021), which calculate the measurement covariance matrix based on the numerical relationship between the measurement error and measurement residual or innovation, respectively. Although the covariance matching methods have a strict mathematical basis, they require that the measurement residual or innovation vectors are of the same dimension at all epochs, which limits their application in the field of satellite navigation and positioning where the number of observations changes with time (Yang & Gao, 2006).

Although a resilient stochastic model can adjust the weights of observations adaptively, the resilient adjustment methods mentioned above are not suitable for PPP. At present, the empirical stochastic models are mainly adopted to determine the weights of observations in PPP. Since the measurement error is the most intuitive manifestation of the measurement accuracy, using the measurement error sequence extracted from the observations to analyze the measurement accuracy should best reflect the true error level of the observations (Zheng & Guo, 2016). In view of this, a resilient adjustment method for pseudorange observation weighting is proposed in this paper. In this method, the real-time estimation model is constructed, which is used to estimate the pseudorange variance based on pseudorange multipath error and measurement noise sequences, to replace the empirical stochastic model for determining the weights of pseudorange observations.

This article is arranged as follows. The observation function model and the empirical stochastic model of PPP are first introduced, and the advantages and disadvantages of the empirical stochastic model are analyzed. Then, the resilient adjustment method and model to establish the pseudorange observation variance are introduced in detail. Afterwards, the performance of the proposed model is evaluated and discussed using the Global Positioning System (GPS) observation data in a static and a dynamic tests. Finally, summary and conclusion are given.

Observation model of precise point positioning

There are two types of observations in PPP, namely pseudorange and carrier phase. Considering the main error items, the pseudorange and carrier phase measurements can be modeled as (Pan, 2018)

$$P_i = \rho + c(\Delta t_r - \Delta t_s) + T_r + I_i + d^i_{\mathrm{MP}} + \varepsilon_i \quad (1)$$

$$L_i = \rho + c(\Delta t_r - \Delta t_s) + T_r - I_i + B_i + d^i_{\mathrm{mp}} + \varsigma_i \quad (2)$$

where i represents the frequency index, c denotes the speed of light in vacuum, P_i and L_i are the pseudorange and carrier phase measurements obtained with a receiver, respectively, ρ is the geometric range between the satellite and the receiver antenna phase centers at emission and reception time, Δt_s is the satellite clock offsets, T_r is the tropospheric delay, I_i is the ionospheric delay, d_{mp} and represent the carrier phase and pseudorange multipath errors, respectively, ε and ς are the pseudorange and carrier phase measurement errors, respectively, Δt_r and B_i are the receiver clock offset and the carrier phase bias, which are unknown parameters.

The error sources affecting the accuracy of observations include satellite orbit and clock errors, atmospheric transmission delay, multipath errors, and measurement noise. Among them, the satellite orbit and clock errors and tropospheric delay can be corrected by models (Guo et al., 2017; Ma et al., 2021; Stpniak et al., 2015). Considering that the ionospheric delay is inversely proportional to the square of the signal frequency, the ionospheric delay can be eliminated by the Ionospheric-Free (IF) observation model as follows (Pan et al., 2021).

$$P_{\mathrm{IF}}(L_{\mathrm{IF}}) = a_i P_i(L_i) - a_j P_j(L_j), a_l = f_l^2 / \left(f_i^2 - f_j^2\right), \quad l \in i,j \tag{3}$$

where P_{IF} and L_{IF} are IF pseudorange and carrier P_{IF} phase observations, which are a linear combination of the pseudorange and carrier phase observations on frequencies f_j and f_i, respectively. However, multipath error and measurement noise are difficult to model and usually cannot be eliminated (Seepersad & Bisnath, 2015; Lau, 2017; Zhang et al., 2018). They are the main factors that reduce the accuracy of observations, especially in a complex environment such as urban.

Empirical stochastic model

The classical method to weigh the observations is to use an empirical stochastic model to estimate the observation variance. Assuming that each error source obeys a Gaussian normal distribution with zero mean, and considering the contributions of all error sources, the observation variance for each satellite in view can be obtained as (Dovis et al., 2015)

$$\sigma_i^2 = \sigma_{\mathrm{clk\&epch},i}^2 + \sigma_{\mathrm{trop},i}^2 + \sigma_{\mathrm{ion},i}^2 + \sigma_{\mathrm{MP},i}^2 + \sigma_{\mathrm{noise},i}^2 \tag{4}$$

where σ_i is the standard deviation of the measurement to the ith satellite. The details of the other symbols are as follows:

- $\sigma_{\mathrm{clk\&eph}}$ is the standard deviation of the satellite clock and orbit errors, which is usually referred to User Range Accuracy (URA) (Bijjahalli & Sabatini, 2021). With broadcast ephemeris, the typical value of URA is 2.4 m, while with precise orbit and clock products, the URA is generally several centimeters or better (Guo et al., 2017).
- σ_{trop} is the standard deviation of troposphere correction model. Because the troposphere delay correction error is mainly caused by the hydrostatic delay σ_{TVE} correction model error, the standard deviation of troposphere delay is modeled by (Dovis et al., 2015)

  $$\sigma_{\mathrm{trop}} = \sigma_{\mathrm{TVE}} \cdot M_{\mathrm{dry}}(\beta_{\mathrm{EL}}) \tag{5}$$

  where σ_{TVE} is the standard deviation of the zenith troposphere delay, which is set to an empirical value 0.12 m, $M_{\mathrm{dry}}(\beta_{\mathrm{EL}})$ is the dry mapping function, and β_{EL} is the satellite elevation angle.
- σ_{ion} denotes the standard deviation of the ionosphere correction model. For a dual-frequency or multi-frequency receiver, the ionospheric delay can be eliminated by dual-frequency IF linear combination, so the standard deviation of ionospheric delay can be set to $\sigma_{\mathrm{ion}} = 0$.
- σ_{noise} is the receiver noise standard deviation. Because receiver measurement noise has random characteristics, it is difficult to model and eliminate it, and the noise characteristics can only be determined by statistical analysis. Researchers have proposed many stochastic models for estimating receiver noise standard deviation. Those stochastic models are generally a function of satellite elevation angle or Signal to Noise Ratio (SNR) (Parvazi et al., 2020). Among them, the sine stochastic function model based on satellite elevation angle is widely used (Parvazi et al., 2020)

  $$\sigma_{\mathrm{noise}}^2 = \frac{\sigma_0^2}{\sin \beta_{\mathrm{EL}}} \tag{6}$$

  where σ_0 is the nominal value of measurement noise standard deviation. For example, $\sigma_0^{\mathrm{L}} = 0.003$ m for GPS P code pseudorange, and $\sigma_0^{\mathrm{P}} = 0.3$ m for carrier phase observable.
- σ_{MP} is the standard deviation of multipath uncertainty. The multipath error is usually treated as a noise, and an empiric stochastic function model based on the satellite elevation angle similar to the receiver measurement noise is used to estimate the standard deviation of the multipath error (Seepersad & Bisnath, 2015).

The above error model is based on the empirical model, which is simple in its implementation. However, in a complex environment, the empirical model can not reflect the real error level due to the mismatching of error model and the user environment (Dovis et al., 2015). In order to improve the reliability of the estimated Global Navigation Satellite System (GNSS) observation accuracy and the performance of the navigation system in dynamic and complex environments, we propose a resilient adjustment method to estimate the pseudorange variance by constructing a real-time estimation model.

Resilient adjustment method to weigh pseudorange observations

Because multipath error and measurement noise have random characteristics, especially multipath error is much dependent of the user environment, it is usually difficult to accurately estimate the variance using empirical stochastic models, which ultimately reduces the positioning performance of GNSS. Compared with carrier phase observations, pseudorange observations are more severely affected by multipath error and measurement noise. Accurate construction of pseudorange variance is the key to improving the convergence time and

positioning quality of precise point positioning (Seepersad & Bisnath, 2015). Therefore, this paper will mainly focus on the research on resilient adjustment methods to weigh pseudorange observations.

Taking the pseudorange multipath error and measurement noise together as a source of error, Eq. (4) can be rewritten as

$$\sigma_i^2 = \sigma_{\text{clk\&epch},i}^2 + \sigma_{\text{trop},i}^2 + \sigma_{\text{ion},i}^2 + \sigma_{\text{mp\&noise},i}^2 \tag{7}$$

where $\sigma_{\text{mp\&noise},i}$ is estimated in real time based on pseudorange multipath error and measurement noise sequences.

Pseudorange multipath error and measurement noise estimation model

In order to extract the multipath error and measurement noise from pseudorange observations, a Code-Minus-Carrier (CMC) observable is adopted (Blanco & Haag, 2011)

$$P_i - L_i = 2I_i + (d_{\text{MP}}^i - d_{\text{mp}}^i) - B_i + (\varepsilon_i - \varsigma_i) \tag{8}$$

The CMC observations constructed by the above formula also include two times of ionospheric delay and carrier phase multipath error and measurement noise, which in general are much smaller than the pseudorange multith error and measurement noise $\left(d_{\text{mp}}^i \ll d_{\text{MP}}^i \text{ and } \varsigma \ll \varepsilon\right)$, so d_{mp}^i and ς can be neglected. There are two ways to handle the ionospheric divergence. For a single frequency receiver, the ionospheric term can be eliminated by fitting and removing a first or second order curve from the CMC observable (Braasch, 2017). For a dual-frequency receiver, the ionospheric delay can be estimated through the dual-frequency carrier phase linear combination (Seepersad & Bisnath, 2015):

$$2a_j(L_i - L_j) = 2I_i + 2a_j(B_i - B_j + d_{\text{MP}}^i - d_{\text{MP}}^j + \varsigma_i - \varsigma_j) \tag{9}$$

Subtracting Eq. (9) from Eq. (8) and ignoring carrier phase multipath error mp and measurement noise ς, the dual-frequen.y ionospheric delay corrected CMC observable on frequency f_i can be obtained as

$$\begin{aligned} d_{CMC}^i &= P_i - L_i - 2a_j(L_i - L_j) \\ &\approx (d_{MP}^i + \varepsilon_i) - (B_i + 2a_j(B_i - B_j)) \\ &= \overline{d}_{MP}^i - \overline{B}_i \end{aligned} \tag{10}$$

where $\overline{d}_{\text{MP}}^i$ represents the pseudorange multipath error and measurement noise, and $\overline{B}_i$ is the carrier phase ambiguities.

In addition to pseudorange multipath error and measurement noise, the CMC observation model in (10) also contains a constant component associated with phase ambiguities. Assuming that no cycles slip occurs in the carrier phase observations and the mean of multipath error and measurement noise is zero, the pseudorange multipath error and measurement noise can be estimated by (Seepersad & Bisnath, 2015; Zheng & Guo, 2016)

$$\overline{d}_{\text{MP}}^{i,k} = s_{\text{CMC}}^{i,k} - \overline{s}_{\text{CMC}}^{i,k}, \overline{s}_{\text{CMC}}^{i,k} = \text{mean}\left(\sum_{t=k_0}^{k} s_{\text{CMC}}^{i,t}\right) \tag{11}$$

where $\overline{s}_{\text{CMC}}^{i,k}$ is the average of $s_{\text{CMC}}^{i,t}$ from the time $t=k_0$ $_0$of the first epoch or the cycle slip occurs to current time $t=k$, which is the estimation of the carrier phase ambiguities $\overline{B}_i$ and removed to eliminate the constant component.

Real-time estimation model for pseudorange variance

Assuming that the multipath error and measurement noise obey the Gaussian normal distribution with zero mean, the pseudorange variance at the current epoch can be estimated based on the previous multipath error and measurement noise sequences (Wang et al., 2013)

$$\hat{\sigma}_{\text{mp\&noise},k}^2 = \frac{\sum_{k=0}^{N-1} (\overline{d}_{\text{MP}}^{i,k})^2}{N} \tag{12}$$

where N is the number of epochs.

Variance inflation processing

In general, the variance estimated by (12) is very conservative, which cannot be used directly as the pseudorange variance. So, it needs to be enlarged to reflect the pseudorange measurement error more accurately. Considering that the multipath error and measurement noise are related to the satellite elevation angle, the following model based on satellite elevation angle is adopted

$$\overline{\sigma}_{\text{mp\&noise},k}^2 = \frac{(s \cdot \hat{\sigma}_{\text{mp\&noise},k})^2}{\sin \beta_{\text{EL}}} \tag{13}$$

where $\overline{\sigma}_{\text{mp\&noise},k}^2$ is the enlarged variance of pseudorange multipath error and measurement noise, and s is the amplification coefficient, which can be set to 2.0–3.0 (Yang & Gao, 2006).

Variance robust estimation

Since the multipath error is very susceptible to the surrounding environment, in dynamic situations, the changes in the surrounding environment sometimes cause sudden changes in multipath errors. In order to reduce the influence of the multipath error mutation on the $\hat{\sigma}_{\text{mp\&noise}}$, it needs to be detected and processed.

Taking the mutation of the multipath error as an abnormal disturbance, the following hypothesis test is constructed (Zhang et al., 2019a, b)

$$H_0 : r \le T, H_1 : r > T \tag{14}$$

where r is test statistic, H_0 is the null hypothesis that there is no multipath and H_1 is the alternative hypothesis that there is a multipath abnormal disturbance. The multipath abnormal disturbance is detected by comparing the magnitude relationship between the test statistic r and the test threshold T.

Under normal circumstances, the measurement variances at adjacent epochs should be similar. So, in order to simplify the processing, the multipath error and measurement noise can be simply regarded as a Gaussian normal distribution with a mean of zero and a variance of $\overline{\sigma}^2_{\text{mp\&noise}}$, and the test statistics can be formulated as

$$r = \frac{\overline{d}^{i,k}_{\text{MP}}}{\overline{\sigma}_{\text{mp\&noise},k-1}} \sim \text{N}_{1-a/2}(0,1) \tag{15}$$

where a is the significance level. The detection threshold T is determined by the significance level a and can be obtained from the standard normal distribution table.

According to the above detection method, if multipath abnormal disturbance is detected, the Huber weight function model is used to adjust the variance of pseudorange multipath error and measurement noise as

$$\tilde{\sigma}^2_{\text{mp\&noise}k} = \overline{\sigma}^2_{\text{mp\&noise},k-1} \cdot \begin{cases} 1 & |r| \le T_0 \\ \frac{T_0}{|r|} & |r| > T_0 \end{cases} \tag{16}$$

where $\tilde{\sigma}^2_{\text{mp\&noise},k}$ is the updated variance of multipath errors and noise, and T_0 is the threshold, which can be set to $T_0 = 1.0$ (Yang & Gao, 2006).

In addition, when a cycle slip occurs in the carrier phase observations or the signal is blocked, the constant component associated with phase ambiguities need to be recalculated. At this time, the $\overline{d}_{\text{MP}}$ is inaccurate in general. In order to avoid the influence of inaccurate $\overline{d}_{\text{MP}}$ on the variance estimation $\hat{\sigma}^2_{\text{mp\&noise}}$, the estimation of $\overline{d}_{\text{MP}}$ at the time of the cycle slip is not involved in the calculation. The processing of real-time estimation of pseudorange variance is shown in Fig. 1.

Figure 2 illustrates an example of the results of pseudorange variance estimation of $\hat{\sigma}^2_{\text{mp\&noise}}$, $\overline{\sigma}^2_{\text{mp\&noise}}$ with inflation processing, and $\tilde{\sigma}^2_{\text{mp\&noise}}$ with inflation processing and robust estimation. The results show that the pseudorange variance estimation obtained by the proposed real-time estimation model is more consistent with the contour of pseudorange error. Since the proposed real-time estimation model takes into account the influence of the surrounding environment on measurement noise and multipath errors, it can obtain a more accurate estimation of the pseudorange variance and provide better estimation of the pseudorange error level than the empirical stochastic model.

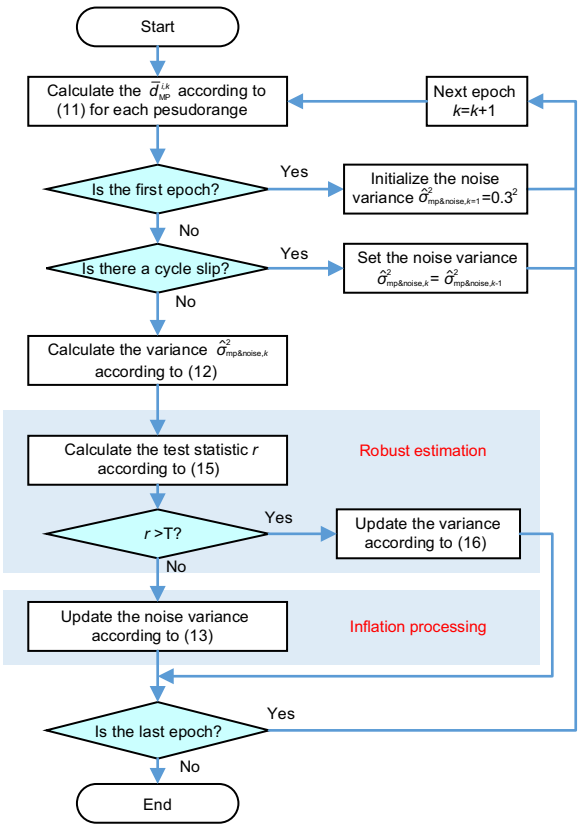

Fig. 1 The processing of real-time estimation of pseudorange variance

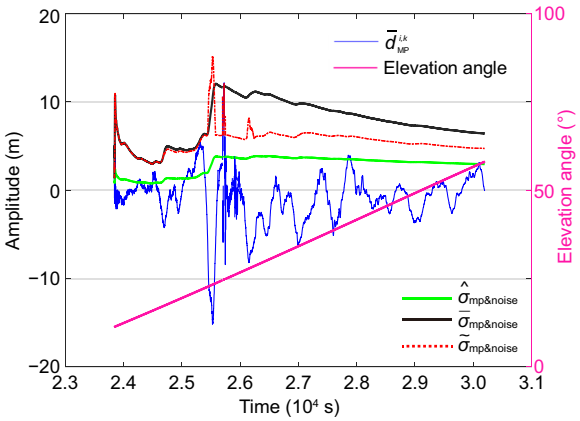

Fig. 2 An example of estimation results of pseudorange variance

Experiment and analysis

In this section, two tests were conducted using a set of static data and a set of ship-borne dynamic data to evaluate the performance of the real-time estimation model. In each test, we first analyzed and compared the estimation accuracy of the real-time estimation model and the empirical stochastic model. To this end, the following three weighting schemes for pseudorange observations are designed:

Scheme 1: The empirical model is adopted, the parameter σ_0 in (6) is set to a general value, $\sigma_0 = 0.3$. (the general empirical model)
Scheme 2: The empirical model is adopted, the parameter σ_0 in (6) is set to the optimal value, which is obtained through post-processing analysis. (the optimal empirical model)
Scheme 3: The real-time estimation m.del is adopted, and the amplification coefficient is set to $s = 3.0$. (the real-time estimation model)

The performance of the real-time estimation model was analyzed from the perspective of the positioning domain by comparing the positioning accuracy and convergence time of kinematic PPP. The positioning accuracy is described by the Root Mean Square (RMS) of positioning errors, which is calculated by

$$s_{\mathrm{RMS}} = \sqrt{\frac{\sum_{i=1}^{n} (\hat{x}_i - x_{\mathrm{ref},i})^2}{n}} \tag{17}$$

where $\hat{x}$ and x_{ref} are the state estimate and reference, and n is the number of epochs. The convergence time is measured as the time until the positioning error in the three directions of East (E), North (N) and Up (U) directions are all less than 0.5 m, which continues for 1 h. The detailed processing strategies of PPP are listed in Table 1.

Tests with static data

The static test data was collected from 00:00:00 to 08:23:16 on Jan 07, 2019 (GPS time) by the C200-AT high-precise GNSS receiver produced by BDStar Navigation company at a sampling frequency of 1 Hz. The receiver antenna was placed on the top of a building, and its surrounding environment is shown in Fig. 3. The coordinates of the station is (− 2 610 957.4 m, 4 232 178.5 m, 3 980 666.8 m) in Earth-Centered Earth-Fixed (ECEF) coordinate system, which is calculated by Canadian Spatial Reference System (CSRS) PPP (Tétreault et al., 2005). The sky plot of visible GPS satellites is shown in Fig. 4, and the number of visible satellites in the test period is 15. It should be noted that due to the long connecting cable (about 50 m) between the receiver and antenna, and the high-rise buildings around the antenna, and the serious multipath errors, the quality of the static observation data is not very good. For this test, the parameter σ_0 of the empirical model in Scheme 2 is set to the optimal value of 1.5 m.

Evaluation of variance estimation

Figure 5 shows the RMS of pseudorange measurement residuals and the standard deviation estimates at each

Table 1 PPP processing strategy and models (Elmezayen and El-Rabbany 2020)

Index	Items	Processing strategy
1	Navigation constellation	GPS only
2	Satellite orbit and clock	Multi-GNSS precise product 'GBM' from GeoForschungsZentrum (GFZ): precise satellite orbit (15 min) and clocks (30 s)
3	Elevation mask angle	7.5°
4	Estimation method	Extend Kalman filtering (EKF)
5	Observation model	IF model
6	Processing mode	Kinematic without dynamics
7	Weighting schemes	Pseudorange: Scheme 1, Scheme 2 and Scheme 3 Carrier-phas using the general empirical model, the parameter is set to $\sigma_0 = 0.003$m.
8	Receiver clock offset	Estimated, modeled as white noise process with a spectral density 1×10^2 m^2/s
9	Satellite and receiver antenna center offset	Corrected by igs14_2035.atx antenna file
10	Phase wind-up	Corrected by model (Pan, 2018)
11	Site displacements	Solid Earth tide, ocean tide, pole tide (Pan, 2018)
12	Tropospheric zenith delay	Hydrostatic delay: using Saastamoinen model and NMF mapping functions model Wet delay: modeled as a random walk process with a spectral density of 1×10^{-5} m^2/s
13	Ambiguity parameter	Float solutions, modeled as constants
14	Relativity effect	Corrected by model (Pan, 2018)

Fig. 3 Sounding environment where the receiver antenna is located

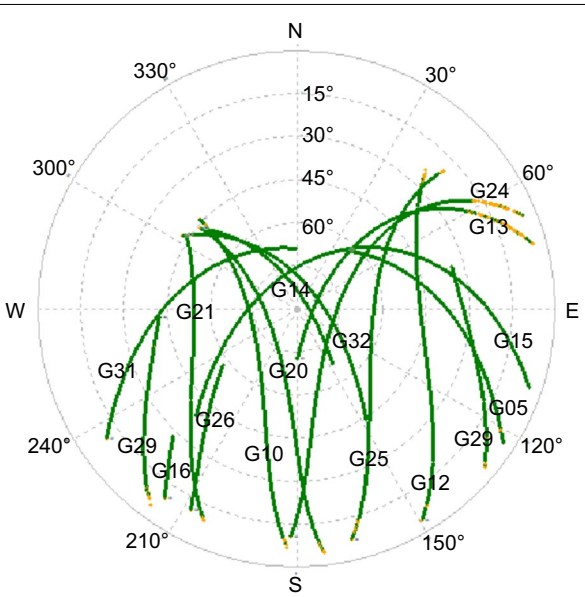

Fig. 4 GPS visible satellite sky plot of static test

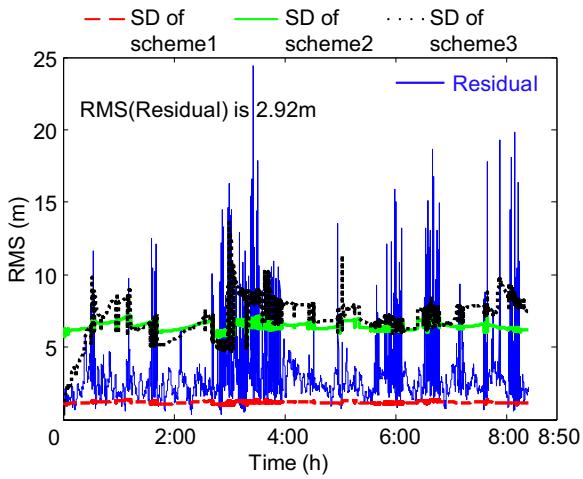

Fig. 5 RMS of pseudorange measurement residuals and standard deviation estimates

epoch. Figure 6 illustrates the pseudorange measurement residuals and standard deviation for each observed satellite. In figures, the blue curve represents the pseudorange measurement residuals. The red, green, and black curves represent the pseudorange Standard Deviations (SD) estimated by the general empirical model in Scheme 1, the optimal empirical model in Scheme 2, and the real-time estimation model in Scheme 3, respectively. The statistical results for each satellite are listed in Table 2.

It can be seen from Figs. 5, 6, and Table 2 that the standard deviation of pseudorange estimated by the general empirical model in Scheme 1 is very conservative, and the average standard deviation is about 1.19 m, which cannot reflect the true error level of the pseudorange observations. The average pseudorange standard deviation calculated by the optimal empirical model in Scheme 2 and the real-time estimation model in Scheme 3 are 6.69 m and 8.01 m, respectively. The standard deviation of pseudorange obtained by these two models are very close to each other, and they can obtain more accurate evaluation results. The statistical results in Table 2 show that the average pseudorange standard deviation estimated by the optimal empirical model and the real-time estimation model is about 2 to 3 times the RMS of pseudorange measurement residuals. In addition, it can be seen from the graph of the pseudorange measurement residuals for each satellite in Fig. 6 that the pseudorange measurement residuals are correlated with satellite elevation angles, and the measurement residuals decrease as the satellite elevation angles increase.

Evaluation of Positioning performance

Figure 7, 8 and 9 show the positioning errors in E, N, and U directions, respectively. Table3 lists the statistical results of the 2 Double (2D) RMS of positioning errors in East (*E*),North (*N*) and Up (*U*) directions and the convergence time.

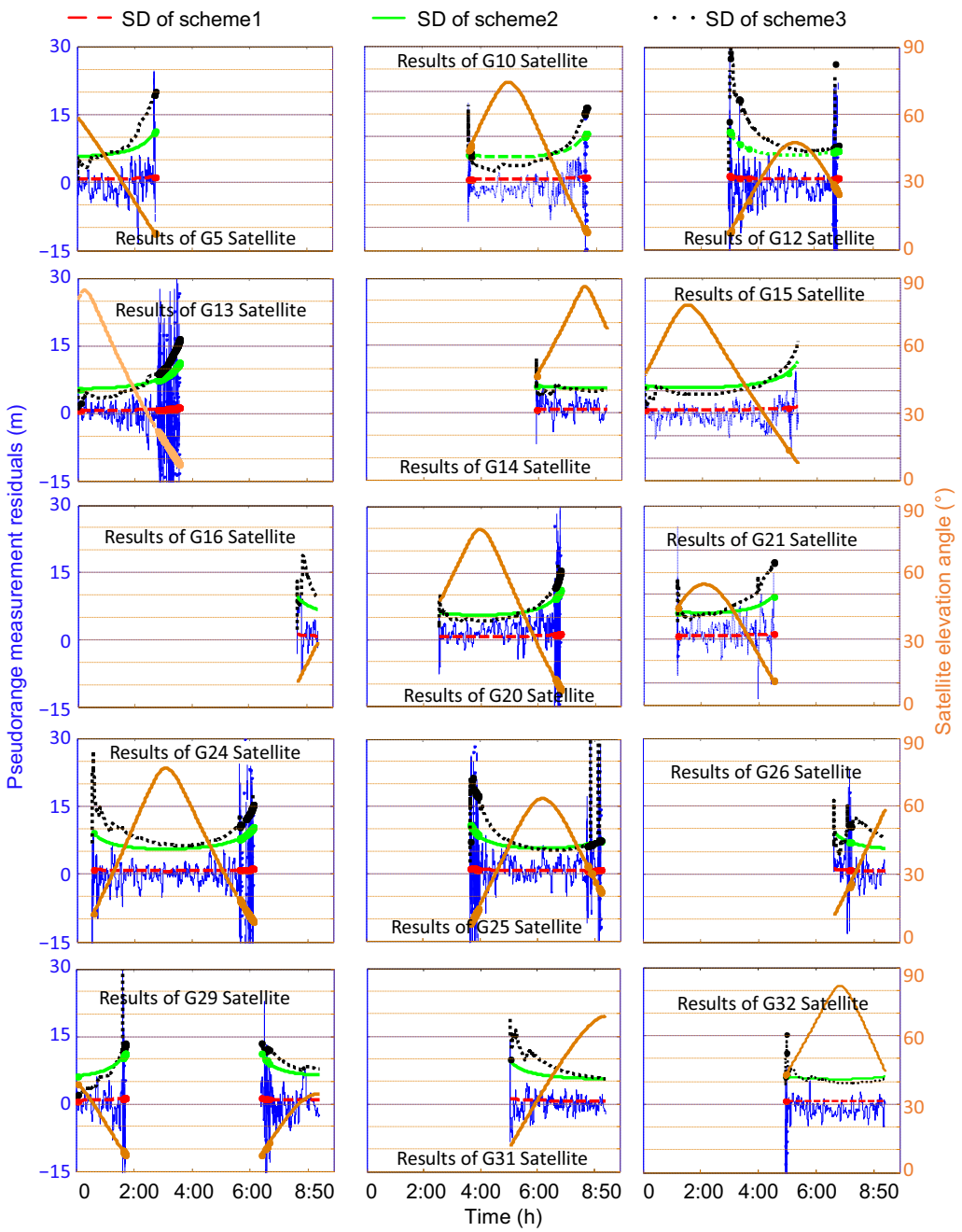

Fig. 6 Pseudorange measurement residuals and standard deviation estimates for each satellite

As can be seen from Figs. 7, 8, 9, the convergence time of PPP using the optimal empirical model in scheme 2 and the real-time estimation model in scheme 3 are better than that of the general empirical model in scheme 1, and the positioning results of PPP using the optimal empirical model and the real-time estimation model are more accurate and stable. It can be also seen from the statistical results in Table 3 that the positioning accuracy of PPP using the general empirical model in scheme 1 is the worst, and the convergence can not be reached in the whole process. Compared with the general empirical model in scheme 1, the positioning performance of PPP using the optimal empirical model in scheme 2 and the real-time estimation model in scheme 3 are significantly improved.

The statistical results in Table 3 show that compared with the general empirical mode in scheme 1, the RMSs of PPP using the optimal empirical model in scheme 2 are

Table 2 Statistical results of the of pseudorange measurement residuals and standard deviation estimates for each satellite

GPS Pseudo Random noise (PRN) number	RMS (Residuals)	Average pseudorange standard deviation estimates in different schemes		
		Results of scheme 1 (general)	Results of scheme 2 (optimal)	Results of scheme 3 (real-time)
5	2.78	1.32	7.50	8.14
10	2.52	1.12	6.34	5.43
12	3.80	1.27	7.22	10.2
13	3.55	1.12	6.34	6.38
14	2.00	0.94	5.33	5.00
15	2.02	1.15	6.52	5.71
16	3.70	1.16	9.14	12.0
20	2.85	1.11	6.31	6.02
21	3.09	1.19	6.72	8.03
24	2.69	1.15	6.53	8.64
25	3.40	1.18	6.67	7.61
26	3.39	1.29	7.28	9.41
29	3.50	1.49	8.43	8.67
31	1.85	1.18	6.67	8.48
32	2.12	0.96	5.45	5.43
ALL	2.92	1.19	6.69	8.01

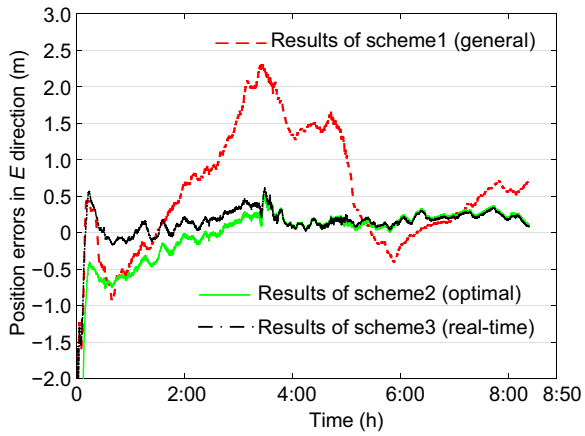

Fig. 7 Position errors in *E* direction

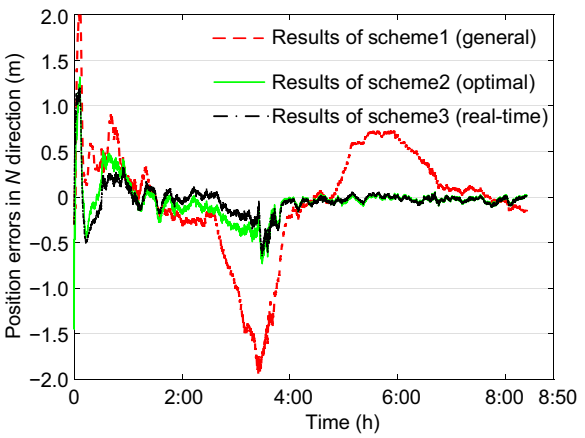

Fig. 8 Position errors in *N* direction

decreased by 0.538, 0.265, and 0.648 m in *E, N, U* directions respectively, and the convergence time is reduced from 30 195 to 4 087 s; the RMSs of PPP using the real-time estimation model in scheme 3 are decreased by 0.616, 0.303, and 0.68 m in *E, N, U* directions respectively, and the convergence time is reduced to 1 964 s. By comparing the positioning results of PPP with scheme 2 and scheme 3, it is found that the positioning performance of PPP with scheme 3 is slightly better than that with Scheme 2. Compared with the optimal empirical model, the real-time estimation model reduces the RMSs of PPP by 0.078, 0.038, and 0.032 m in *E*, *N*, *U* directions respectively, and the convergence time by 2123 s.

In summary, both the optimal empirical model and the real-time estimation model can obtain more accurate pseudorange variance estimates, and therefore can achieve better positioning performance than the general empirical model. Compared with optimal empirical model, the real-time estimation model can adaptively adjust the pseudorange standard deviation estimates according to the changes in the measurement error level at each epoch, so the real-time estimation model can

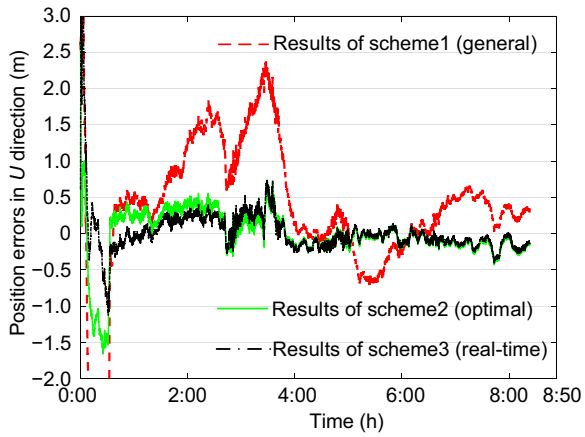

Fig. 9 Position errors in *U* direction

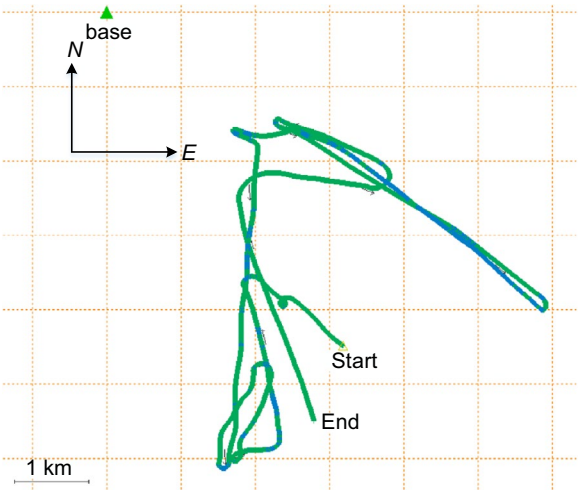

Fig. 10 Ship-borne reference trajectory

better reflect the actual error level of the pseudorange observations at each epoch, and achieve better positioning performance.

Tests with ship-borne dynamic data

To further assess the performance of the real-time estimation model in dynamic environment, a ship-borne test was carried out on January 1, 2019, which lasted for about 3.5 h. The test data was collected by the NovAtel SPAN PwrPak7D-E1 receiver, and the sampling frequency is 1 Hz. Figure 10 shows the reference trajectory, which is calculated by the NovAtel Inertial Explore 8.80 post-processing software through the carrier phase Differential Global Navigation Satellite System (DGNSS) positioning mode, with centimeter-level positioning accuracy. Figure 11 shows the GPS satellite sky plot, the number of visible satellites during the test period is 15. In this test, the parameter σ_0 in Scheme 2 is set to the optimal value of 2.5 m.

Evaluation of variance estimation

Figure 12 shows the RMS of pseudorange measurement residuals and the standard deviation estimates at each epoch. Figure 13 illustrates the pseudorange measurement residuals and standard deviation for each

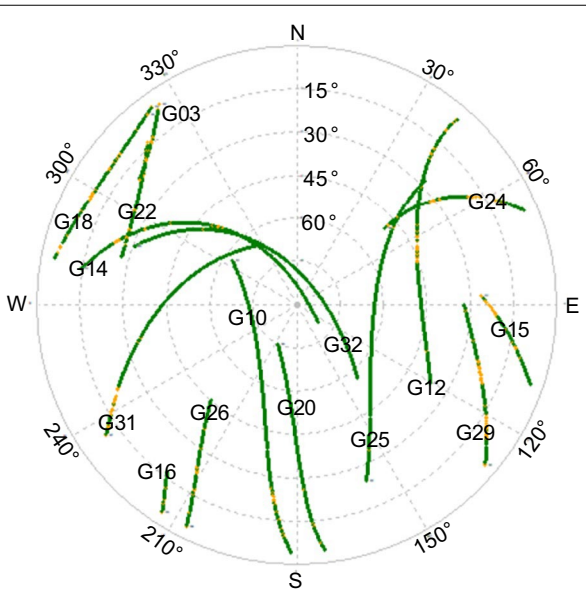

Fig. 11 GPS satellite sky plot of ship-borne dynamic test

Table 3 Statistical results of PPP positioning errors and convergence time based on the static test data

Weighting scheme	2D RMS in different directions (m)			Convergence time (s) (Threshold is 0.5 m)
	East direction	North direction	Up direction	
Scheme 1 (general)	0.828	0.412	0.869	30 195
Scheme 2 (optimal)	0.290	0.147	0.221	4 087
Scheme 3 (real-time)	0.212	0.109	0.189	1 964

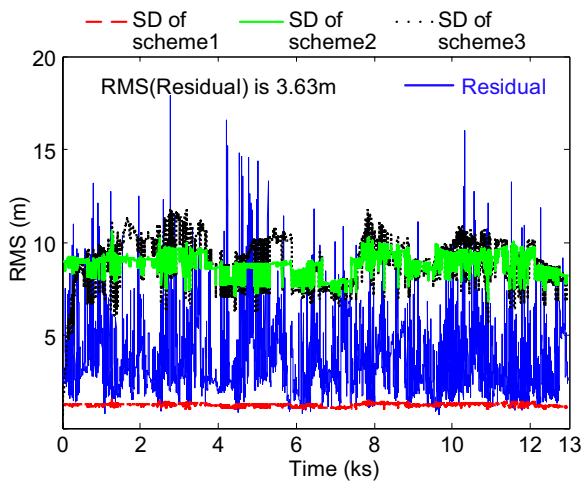

Fig. 12 RMS of pseudorange measurement residuals and standard deviation estimates

satellite. The statistical results for each satellite are listed in Table 4.

It can be seen from the statistical results in Table 4 that the RMS of pseudorange measurement residuals is about 3.63 m, while the average pseudorange standard deviation estimated by the general empirical model in Scheme 1 is about 1.26 m, which is obviously, conservative and cannot reflect the actual error level of pseudorange observations. The average pseudorange standard deviations estimated by the optimal empirical model in scheme 2 and the real-time estimation model in Scheme 3 are 8.84 m and 8.96 m, respectively. They are equivalent, about 2–3 times the RMS of pseudorange measurement residuals. It can be seen that the real-time estimation model and the optimal empirical model have the same estimation accuracy and can better reflect the pseudorange error level.

Evaluation of Positioning performance

The convergence behavior of the positioning for the ship-borne test data in *E*, *N*, *U* directions are illustrated in Figs. 14, 15, 16. The statistical results of positioning errors and convergence time are listed in Table 5.

It can be seen from the position errors graph in Figs. 14, 15, 16 and the statistical results of positioning performance in Table 5 that the positioning results of PPP with Scheme 1 are the worst. This is because the model cannot reflect the actual error level of pseudorange observations. Compared with the model in Scheme 1, the model in Scheme 2 can reduce the positioning RMS of PPP by 0.207, 0.362, and 1.067 m in E, N, U directions respectively, and the convergence time from 12974 to 2225 s; the model in Scheme 3 can reduce the positioning RMS of PPP by 0.269, 0.57, and 1.213 m in *E*, *N*, *U* directions respectively, and the convergence time to 1126 s. The positioning performance of PPP with the optimal empirical model and real-time estimation model has been greatly improved.

Table 4 Statistical results of the RMS of pseudorange measurement residuals and average pseudorange standard deviation estimates for each satellite

GPS PRN	RMS (Residuals)	Average pseudorange standard deviation estimates in different schemes		
		Results of scheme 1(general)	Results of scheme 2(optimal)	Results of scheme 3(real-time)
3	5.28	1.86	13.0	19.4
10	2.74	1.14	7.99	8.00
12	3.78	1.28	8.93	8.97
14	3.01	1.10	7.73	7.03
15	7.73	1.87	13.1	15.5
16	6.90	1.96	13.7	15.7
18	6.37	2.26	15.8	26.0
20	3.65	1.25	8.76	6.61
22	4.54	1.45	10.2	10.9
24	4.32	1.33	9.33	8.81
25	2.27	1.07	7.47	5.72
26	2.92	1.46	10.2	9.52
29	4.16	1.54	10.8	13.4
31	3.50	1.15	8.04	9.22
32	1.97	0.99	6.92	5.55
All	3.63	1.26	8.84	8.96

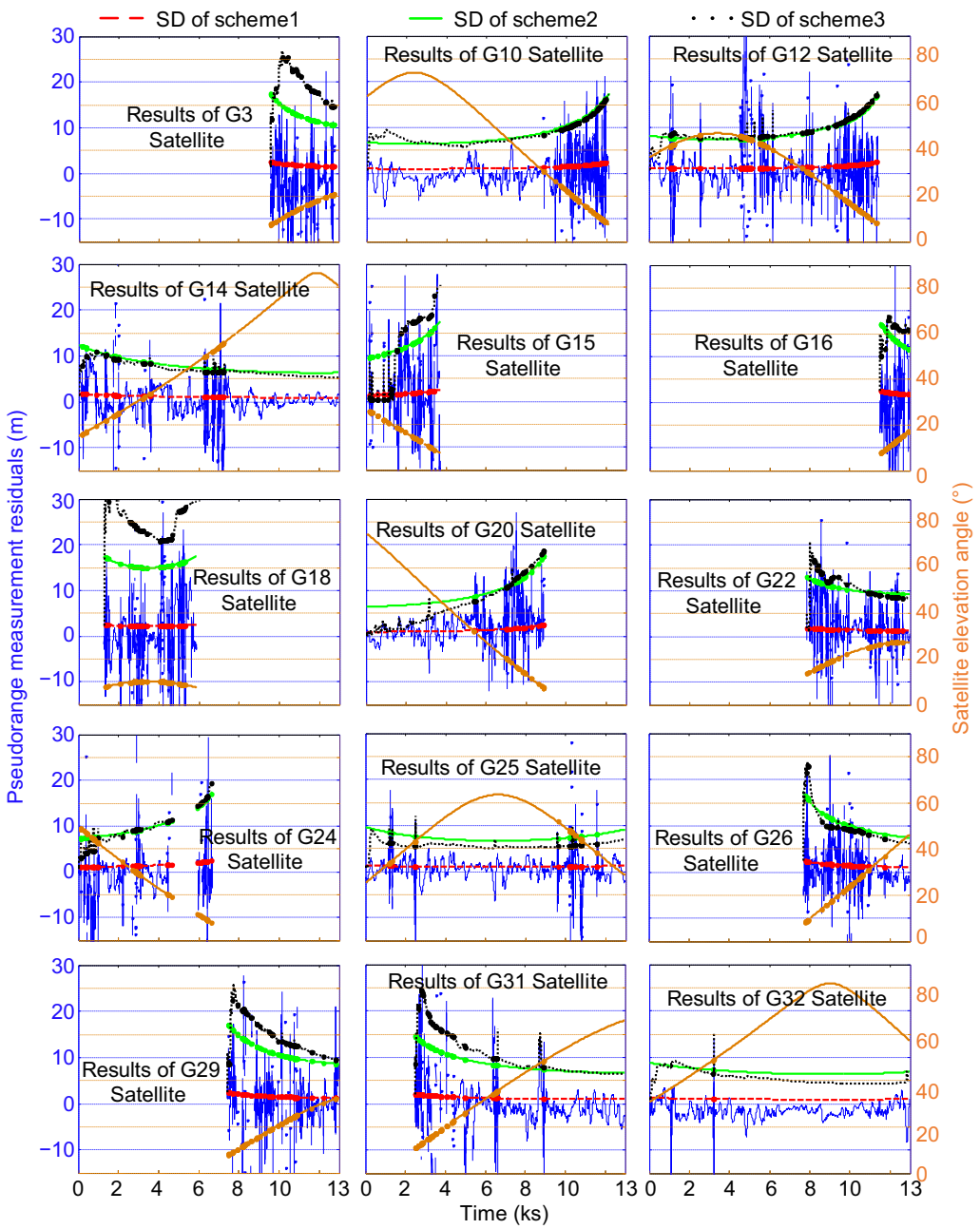

Fig. 13 Pseudorange measurement residuals and standard deviation estimates for each satellite

In addition, compared with the model in scheme 2, the positioning accuracy of PPP with model in scheme 3 is further improved by 0.062, 0.208 and 0.146 m in *E*, *N*, *U* directions directions respectively, and the convergence time is reduced by 1099 s. The positioning performance of PPP with model in scheme 3 is slightly better than that with the model in scheme 2. This is because the real-time estimation model can dynamically adjust the pseudorange standard deviation according to the degree of the influence of surrounding environment on the measurement error, so it can obtain a more accurate estimation than the optimal empirical model.

Conclusions

In this paper, a resilient adjustment method to weigh pseudorange observations is proposed, which constructs a real-time estimation and inflation model for

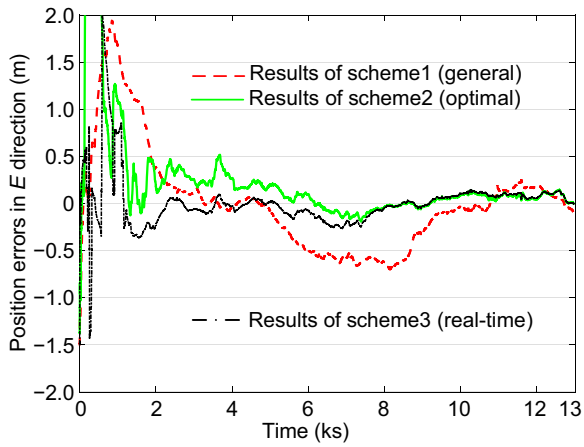

Fig. 14 Position errors in *E* direction

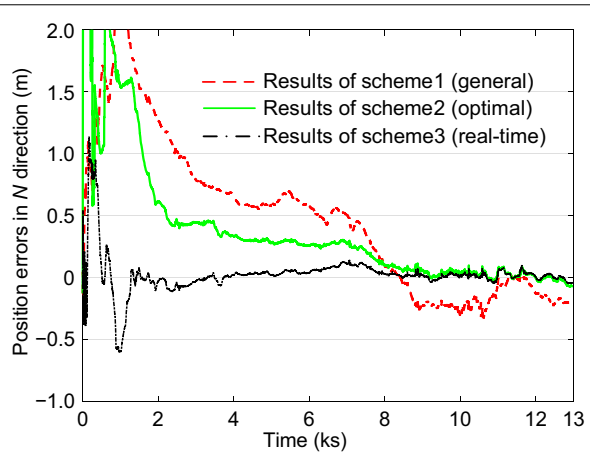

Fig. 15 Position errors in *N* direction

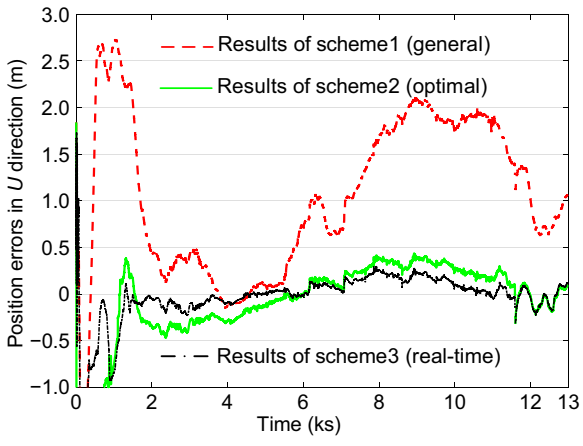

Fig. 16 Position errors in *U* direction

the pseudorange variance of multipath error and measurement noise to deal with the unpredictable and time-varying of pseudorange observation error in a dynamic and complex environment. Since the influence of the surrounding environment on measurement noise and multipath error is considered, the standard deviation of the pseudorange obtained by the real-time estimation model can provide a better representation of the pseudorange error level, and the positioning performance of PPP using the real-time estimation model is better than the empirical stochastic model. The experimental results illustrated that compared with the optimal empirical stochastic model, the positioning accuracy of PPP using the real-time estimation model is improved by at least 20%, and the convergence time is reduced by at least 50%. However, it should be noted that the proposed resilient adjustment method is only suitable for dual-frequency pseudorange observations, and cannot adjust the weight of the carrier phase observations, also the influence of abnormal carrier phase observations cannot be handled. In addition, since ambiguity convergence takes some time, the pseudorange variance estimated by the proposed real-time estimation model may be inaccurate during this period. Carrier phase is another important observation in GNSS. Setting appropriate weights for carrier phase observations is of great significance to improve the positioning reliability and accuracy of PPP. Therefore, how to realize the resilient adjustment of the weight of the carrier phase observation will be one of the further works.

Table 5 Statistical results of PPP positioning errors and convergence time based on ship-borne dynamic test data

Weighting scheme	2D RMS in different directions (m)			Convergence time (s) (Threshold is 0.5 m)
	East direction	North direction	Up direction	
Scheme 1 (general)	0.382	0.621	1.335	12974 s
Scheme 2 (optimal)	0.175	0.259	0.268	2225 s
Scheme 3 (real-time)	0.113	0.051	0.122	1126 s

Acknowledgements
Not applicable.

Author contributions
Zhang Qieqie designed and performed research, and was a major contributor in writing the manuscript. Zhao Long and Zhou Jianhua reviewed and revised the paper. All authors read approved the final manuscript.

Authors' information
Qieqie Zhang, received the Ph.D. degree in control theory and control engineering form Beihang University, Beijing, China. He is currently an associate professor at the college of Automation Engineering, Nanjing University of Aeronautics and Astronautics. His primary areas of interest are integrated navigation systems, particularly the integrated navigation systems involving global positioning system, inertial navigation or both.
Long Zhao, received the Ph.D. degree in precision instrument and machinery from the Beijing University of Aeronautics and Astronautics, Beijing, China, in 2004. He is currently a Professor with the School of Automation Science and Electrical Engineering, Beihang University, Beijing, where he is the Head of the Digital Navigation Center. His research focuses on the inertial navigation, geophysical navigation, vision navigation, and multi-source information adaptive fusion navigation.
Jianhua Zhou, received the Ph.D. degree in geodesy from Nanjing University, Nanjing, Jiangsu, China. She is a Professor with Beihang University, Beijing, China. Her main research activities comprise applications of GNSS, autonomous navigation system, precise orbit determination, and multi-constellation GNSS.

Funding
This work is supported by the National Key Research and Development Program of China (Grant No. 2020YFB0505804), the Fundamental Research Funds for the Central Universities (Grant No. 56XAA22055), National Natural Science Foundation of China (Grant No. 41874034), the Beijing Natural Science Foundation (Grant No. 4202041).

Availability of data and materials
All data generated during the current study are available in this published article and its supplementary information files. The original ship-borne datasets involves commercial interests, which are available from the corresponding author on reasonable request.

Declarations

Competing interests
We understand that our manuscript and associated personal data will be shared with Research Square for the delivery of the author dashboard. We declare that we have no conflicts of interest to this work.

Author details
[1]College of Automation Engineering, Nanjing University of Aeronautics and Astronautics, Nanjing 211106, China. [2]Digital Navigation Center, School of Automation Science and Electrical Engineering, Beihang University, Beijing 100191, China. [3]Beijing Satellite Navigation Center, Beijing 100094, China.

Received: 28 March 2022 Accepted: 22 June 2022
Published online: 08 August 2022

References

Bijjahalli, S., & Sabatini, R. (2021). A high-integrity and low-cost navigation system for autonomous vehicles. *IEEE Transactions on Intelligent Transportation Systems, 22*(1), 356–369.
Blanco, D. N., Haag, M. (2011). Multipath analysis using code-minus-carrier for dynamic testing of GNSS receivers. In: *International conference on localization and GNSS (ICL-GNSS)*, pp. 25–30.
Braasch, M. S. (2017). Multipath. In P. J. G. Teunissen (Ed.), *Global navigation satellite systems* (pp. 443–468). Springer.
Dovis, F., Muhammad, B., & Cianca, E. A. K. (2015). A run-time method based on observable data for the quality assessment of GNSS positioning solutions. *IEEE Journal on Selected Areas in Communications, 33*(11), 2357–2365.
Elmezayen, A., & El-Rabbany, A. (2020). Real-time GNSS precise point positioning using improved robust adaptive Kalman filter. *Survey Review, 53*(381), 528–542.
Gao, Z., Shen, W., Zhang, H., Ge, M., & Niu, X. (2016). Application of Helmert variance component based adaptive Kalman filter in multi-GNSS PPP/INS tightly coupled integration. *Remote Sensing, 8*(7), 553–571.
Guo, F., Li, X. X., Zhang, X. H., & Wang, J. L. (2017). Assessment of precise orbit and clock products for Galileo, BeiDou, and QZAA from IGS Multi-GNSS Experiment (MGEX). *GPS Solutions, 21*(1), 279–290.
Lau, L. (2017). Wavelet packets based denoising method for measurement domain repeat-time multipath filtering in GPS static high-precision positioning. *GPS Solutions, 21*(2), 461–474.
Lee, H., Lee, C., Jeon, H., et al. (2020). Interference-compensating magnetometer calibration with estimated measurement noise covariance for application to small-sized UAVs. *IEEE Transactions on Industrial Electronics, 67*(10), 8829–8840.
Liu, Y. H., Ning, X. L., Li, J. L., et al. (2021). Adaptive central difference Kalman filter with unknown measurement noise covariance and its application to airborne POS. *IEEE Sensor Journal, 21*(8), 9927–9936.
Ma, H. Y., Psychas, D., Xing, X. H., Zhao, Q. L., Verhagen, S., & Liu, X. L. (2021). Influence of the inhomogeneous troposphere on GNSS positioning and integer ambiguity resolution. *Advanced in Space Research, 67*(6), 1914–1928.
Pan, Z. P. (2018). Theory and method of GNSS precise point positioning and its quality control. Master's Thesis, PLA Strategic Support Force Information Engineering University, China.
Pan, L., Gao, X., Hu, J. H., Ma, F. J., Zhang, Z. Y., & Wu, W. W. (2021). Performance assessment of real-time multi-GNSS integrated PPP with uncombined and ionospheric-free combined observables. *Advances in Space Research, 67*(1), 234–252.
Parvazi, K., Farzaneh, S., Safari, A. (2020). Role of the RLS-VCE estimated stochastic model for improvement of accuracy and convergence time in multi-GNSS precise point positioning. *Measurement, 165*, Article 108073.
Seepersad, G., & Bisnath, S. (2015). Reduction of PPP convergence period through pseudorange multipath and noise mitigation. *GPS Solutions, 19*(3), 369–379.
Shen, N., Chen, L., Lu, X., et al. (2022). Interactive multiple-model vertical vibration detection of structures based on high-frequency GNSS observations. *GPS Solutions, 26*(2), 48–66.
Stpniak, L., Bogusz, J., Klos, A., Wielgosz, P. (2015). Assessment of tropospheric delay estimation methods on Precise Point Positioning time series. In: *26th international union of geodesy and geophysics*, Prague, Czech.
Tétreault, P., Kouba, J., Héroux, P., et al. (2005). CSRS-PPP: An internet service for GPS user access to the Canadian Spatial Reference Frame. *Geomatica, 59*(1), 17–28.
Wang, L., Feng, Y., & Wang, C. (2013). Real-time assessment of GNSS observation noise with single receivers. *Journal of Global Positioning Systems, 12*(1), 73–82.
Yang, Y. (2019). Resilient PNT concept frame. *Journal of Geodesy and Geoinformation Science, 2*(3), 1–7.
Yang, Y., & Gao, W. (2006). An optimal adaptive Kalman filter. *Journal of Geodesy, 80*(4), 177–183.
Zhang, H. Y., Ji, S. Y., Wang, Z. J., & Chen, W. (2018). Detailed assessment of GNSS observation noise based using zero baseline data. *Advances in Space Research, 62*(9), 2454–2466.
Zhang, L., Sidoti, D., Bienkowski, A., et al. (2020). On the identification of noise covariances and adaptive Kalman filtering: A new look at a 50 year-old problem. *IEEE Access, 8*, 59362–59388.
Zhang, Q. Q., Zhao, L., & Zhou, J. H. (2019a). A novel weighting approach for variance component estimation in GPS/BDS PPP. *IEEE Sensors Journal, 19*(10), 3763–3771.
Zhang, Q. Q., Zhao, L., & Zhou, J. H. (2019b). Improved method of single and multiple GNSS faults exclusion based on consensus voting. *The Journal of Navigation, 74*(2), 1–20.

Zheng, J. Z., & Guo, F. (2016). An adaptive stochastic model for GPS observations and its performance in precise point positioning. *Empire Survey Review, 48*(349), 296–302.

Publisher's Note